Write-Read 3D Patterning with a Dual-Channel Nanopipette

Dmitry Momotenko,[1,] Ashley Page,[1,2] Maria Adobes-Vidal[1] and Patrick R. Unwin[1,*].*

[1]Department of Chemistry and [2]MOAC Doctoral Training Centre, University of Warwick, Coventry, CV4 7AL, United Kingdom

*p.r.unwin@warwick.ac.uk

*d.momotenko@warwick.ac.uk

ABSTRACT

Nanopipettes are becoming extremely versatile and powerful tools in nanoscience for a wide variety of applications from imaging to nanoscale sensing. Herein, the capabilities of nanopipettes to architect and build complex free-standing three-dimensional (3D) nanostructures are demonstrated using a simple double-barrel nanopipette device. Electrochemical control of ionic fluxes enables highly localized delivery of precursor species from one channel and simultaneous (dynamic and responsive) ion conductance probe-to-substrate distance feedback with the other for reliable high-quality patterning. Nanopipettes with 30–50 nm tip opening dimensions of each channel allowed confinement of ionic fluxes for the fabrication of high aspect ratio copper pillars, zigzag and Γ-like structures, as well as permitting the subsequent topographical mapping of the patterned features with the *same nanopipette probe* as used for nanostructure engineering. This approach offers versatility and robustness for high resolution 3D "printing" (writing) and read-out at the nanoscale.

KEYWORDS

Scanning ion conductance microscopy, nanopipette, electrodeposition, electrochemical imaging

Three-dimensional (3D) micro- and nanostructures can offer unique and intriguing physical and optical properties that find applications in numerous research and technology disciplines spanning electronics,[1] sensing and analysis,[2] biotechnology and biomedicine,[3] tissue engineering,[4] nanoscale motion devices[5] and many others. The fabrication of 3D objects with a high degree of control over shape and size, however, still presents many challenges. Techniques that enable 3D patterning include template methods[6,7] (typically, lithography followed by an appropriate way of filling cavities in a resist, *e.g.* electroplating, physical or chemical vapour deposition *etc.*), electron- and ion beam-induced structuring[8,9] that allow modification of surfaces using precursors from gas or liquid phases, self-assembly (based on, for instance, DNA strains as building blocks[10] or DNA origami[11]) and scanning probe microscopy (SPM) methods. The family of SPM techniques offers powerful capabilities for the direct manipulation of matter at the tip of the probe, and on the fabricated object, with no need for a mask or template. This opens up single step processing, without post-fabrication operations on the patterned structures, as well as providing high versatility, as SPMs enable operation in gas and liquid environments and under vacuum.[12] Surface modification with SPMs is possible in many different ways, including the manipulation of "building blocks" such as nanoparticles,[13,14] deposition in a layer-by-layer fashion,[15] local removal of material by scratching or thermal desorption,[16] modification of local environment using ultramicroelectrodes,[17-19] or confined delivery using, for example, micro- and nanopipette probes.[1,13,20-31] Approaches using multiplexed probes, such as microelectrode

arrays,[32] multiple cantilevers for atomic force microscopy (AFM)[33,34] and dip-pen lithography,[35] for high-throughput patterning have also been developed, ~~allowing to overcome issues attributed to a typically slow~~ which offer great opportunities to speed up probe-based fabrication processes.

Nanopipettes are particularly useful tools in nanoscience as they allow the precise spatiotemporal control, analysis and manipulation of material fluxes.[36,37] Most recently nanopipettes have proven powerful as probes for multifunctional imaging, as exemplified by simultaneously mapping topography and reactivity,[36,38,39] and for probing heterogeneously distributed surface charge magnitudes alongside topography.[40-42] We develop this multifunctional capability herein, demonstrating 3D writing and reading with nanopipette probes.

For nanofabrication purposes, nanopipettes filled with electrolyte can serve as a local reservoir of desired molecules/ions for deposition and can therefore provide a highly localized flux of species towards the substrate. Nanopipettes enable surface modification both in electrolyte solution[22,23,27] and in a scanning droplet cell configuration,[21,43,44] and the deposition of metals from precursors and nanoparticle dispersions has been shown for the fabrication of complex planar and 3D features at interfaces.[1,13,24,25,30,45,46] However, the main difficulty in fabricating arbitrary 3D shapes is the issue of controlling the probe-to-substrate distance during deposition (positional feedback). This is a crucial aspect, as it affects the quality of the deposited structures. Recently, these issues were addressed by the implementation of hollow microfluidic AFM cantilevers, so-called FluidFM probes,[47] which enabled the microscale fabrication of complex 3D objects by electroplating copper. The deposition occurred under the aperture of an AFM tip with simultaneous force control of tip-to-substrate distance, as well as accurate regulation of electrolyte flow by physically flowing solution through the hollow AFM tip.[48,49]

Herein, we demonstrate the deposition of complex high aspect ratio objects using simultaneous electrochemical delivery and distance control, with a simple dual-barrel nanopipette probe. This approach to 3D patterning achieves higher resolution than presently possible with AFM devices, and is accomplished without any need for flow systems. In addition, nanopipette probes allow the read-out of the resulting patterns using the topographical mapping capabilities of scanning ion conductance microscopy (SICM)[50] with the same dual probe.

RESULTS AND DISCUSSION

Operational principle

High quality 3D patterning at an interface with a probe-based technique requires simultaneous responsive control of the probe-to-substrate distance and accurate on-demand delivery of material to the substrate. This can be implemented by using a dual-barrel nanopipette in which one of the nanopipette barrels is a local source of precursor material while the other is used for local ion conductance measurements in an SICM setup, providing feedback for precise probe positioning.[50,51] Herein, this concept is demonstrated for the electrodeposition of copper structures using the setup shown in Figure 1a. This configuration allows: i) independent control of electrochemical potential on the gold thin film substrate for copper plating (or stripping, if desired) via E_{sub} and V_{ref}; ii) regulation of ion flow through the SICM nanopipette barrel, used for distance feedback and induced by the potential difference, V_{ref}, between the quasi-reference counter electrodes (QRCEs) in the nanopipette and solution bulk; and iii) management of the Cu^{2+} ion flux through the other nanopipette barrel, determined by the applied bias value ($V_{delivery}$-V_{ref}) to the QRCE in the pipette, used for local delivery of precursor species. Importantly, the applied potentials in ~~such~~ this setup ~~configuration~~ are controlled independently and simultaneously (with the aid of specifically designed LabVIEW code in combination with the

hardware), and all the potentials are reported with respect to the QRCE in the solution bulk. In this way, for the engineering of 3D features at interfaces, there is very fine control of the deposition rate (via both the applied substrate potential and regulation of the Cu^{2+} flow current by the applied bias), coupled with the maintenance of a constant probe-to-substrate distance, enabling automatic probe retract as a feature grows, ensuring high quality patterning. SICM feedback was induced by a constant DC bias (in the range ±0.2 V, except of the example shown in Figure 3a where the SICM bias was set to -0.25 V, *vide infra*). The possibility to control the nanopipette bias polarity ~~in some cases c~~ould~~an~~ be beneficial for the technique operation, for example to prevent the ~~especially, if the deposited material can contain charged nanoparticles that can migrate (due to the imposed high electric field) towards the~~ nanopipette tip ~~and~~ from clogging, ~~or stick to it, causing perturbation of ionic fluxes (however,~~although this is not the case for copper deposition exemplified herein~~).~~

An important attribute of nanopipette methods is the simplicity and the low cost of probe fabrication, especially when compared to probe manufacture for other SPMs: pulling capillaries with diameters that are highly tuneable, and range from tens of microns down to a few nanometers is a simple and routine task, that does not require any special facilities (except a laser pipette puller). This is an important consideration, as the size of the nanopipette probe is a factor determining both the mass transport rates through the nanopipette orifice[52] and the lateral dimensions of the deposit; the smaller the probe, the higher the confinement of the reagent flow and thus the smaller the lateral dimension of the patterned feature. Figure 1b is a TEM image of a typical dual-barrel nanopipette employed herein for patterning of high-aspect ratio copper structures. The overall pipette tip diameter (taking into account the thickness of glass walls that reaches 14 nm at the tip) is about 120 nm, whereas the opening dimensions of each of the

nanopipette barrels are around 30 – 50 nm. This is about an order of magnitude smaller than the opening size of FluidFM probes (300 nm – 1 μm) recently employed for patterning of free-standing 3D copper microstructures.[49]

Patterning

Figure 2 demonstrates the evolution of probe position as well as DC ion current and AC amplitude (used as feedback) during a typical deposition experiment used to produce a Cu tower on a substrate. Prior to patterning, the nanopipette approaches the gold substrate (region marked "I" in Figures 2a and b) until the AC amplitude (due to the oscillation of the probe normal to the substrate) reaches a specified feedback set point (1.5 pA in the case of Figure 2), indicating close proximity of the probe to the sample interface; see Experimental section. During the approach the pipette barrel that contains Cu^{2+} ions is biased at a slightly negative potential (value between -0.1 to -0.3 V) to ensure minimum precursor (Cu^{2+}) flux towards the substrate. As the nanopipette reaches the approach set point, typically corresponding to a distance of slightly more than the nanopipette opening radius from the interface, the bias at the QRCE in the precursor-containing probe barrel is changed to a certain positive value (with respect to QRCE in solution bulk), driving copper ions through the nanopipette opening for local delivery. A sudden change of ion flux in the probe-to-substrate gap due to the rapid switch in bias causes a spike in both the DC and AC ion current through the barrel employed for SICM distance control, leading to the fast retract of the pipette by a few hundred nanometers (at a time of ca. 35 s in the region marked "II" in Figures 2a and b) before reapproaching to the set point distance as the current spike flattens out. After this short period (usually, a few hundreds of ms long), positional feedback stabilizes the probe above the substrate (also during region "II"). As the deposition process starts,

promoted by the bias applied to the substrate electrode (*vide infra*), SICM automated positioning maintains a constant probe-to-substrate distance by a slow retract of the probe due to the feature growth underneath the nanopipette orifice (Figures 2a and b, marked "III"). The automated positioning uses a feedback loop with a specified update time (typically 50 ms herein, but tuneable), which compares the AC amplitude to the desired set point, adjusting the tip position accordingly. In the example shown in Figure 2, a 4.8 μm height pillar was deposited in 60 s, with an average deposition rate of about 80 nm s^{-1} as evidenced by a reasonably constant rate of probe retract. Interestingly, the deposition of the first ~100 nm (on Figures 2a and b, marked as "II") of the feature usually occurs at a lower rate (in this example, about 20 nm s^{-1}), which is likely to be related to the substrate capture area of reagent flow. When the probe is positioned above a planar substrate, deposition can occur over a large surface area. However, as the feature grows under the nanopipette probe the deposition current becomes more focused on the smaller area at the growing end of the deposit, leading to a stable and confined patterning of freestanding structures.

Figure 3a demonstrates the importance of the substrate potential, E_{sub}, on the patterning quality. Herein, the substrate was held at a constant potential throughout ~~all~~ the entire experimental routine, from the initial probe approach and until the end of the deposition. However, it would be~~is~~ possible to vary the substrate potential during depositions without significant influence on the feedback (unless the potential wa~~i~~s stepped sharply to another value, that could~~an~~ cause a spike in the DC and AC pipette currents and hence a retraction of the pipette ~~retract~~ for a short period of time due to the feedback mechanism). Typically, copper deposition starts at about -0.3 to -0.4 V *vs.* Ag/AgCl QRCE. However, at a low deposition overpotential (-0.4 V) the kinetics of deposition is sluggish and so the collection of the delivered Cu^{2+} ions at the substrate occurs over a large substrate area leading to rather unconfined electrodeposition, from

which 3D features evidently cannot be constructed on this timescale. At larger electroplating driving forces (E_{sub} = -0.5 to -0.7 V) the patterns start exhibiting more pillar-like structures as the increased overpotential significantly enhances the local deposition rate leading to a more confined collection of the precursor (Cu^{2+} reduction to Cu) at the substrate directly underneath the nanopipette probe. The increase of the substrate overpotential, E_{sub}, also results in a faster growth of the features; the deposition rate gradually increases from an average of ~2 nm s^{-1} (-0.4 V) to 21 nm s^{-1} (-0.5 V) and then to 29 and 66 nm s^{-1} (-0.6 and -0.7 V, respectively), allowing the construction of taller pillars within the fixed deposition time considered (180 s). These data highlight that for a given Cu^{2+} flux from the nanopipette, the substrate potential ultimately determines the upper limit of the deposition rate, which otherwise is controlled by the magnitude of Cu^{2+} flow to the substrate (determined by the bias value applied to the QRCE in the nanopipette delivery channel). Importantly, the diffusional flux (0 V bias applied to the copper-containing barrel) ~~cannot~~ does not provide sufficiently high ~~enough~~ mass transport of Cu^{2+} towards the substrate and therefore does not result in the~~a~~ deposition of features (at least, within a timescale considered). At larger driving potential, the migration of ions in the electric field dominates the mass transport and can result in much higher deposition rates and taller pillars (Figure 3a). Furthermore, the flux of ~~copper~~ Cu^{2+} ions can be controlled ~~depending on~~by the precursor concentration: the higher the concentration of Cu^{2+} ~~amount~~ in the electrolyte ~~is~~, the lower the bias value ~~is~~ required to drive the flow of ~~copper~~ Cu^{2+} towards the substrate at a ~~certain~~ given rate. The overall quality of the deposits (feature thickness, shape and roughness) appears consistent under inspection by SEM and is not significantly influenced by the bias value that drives Cu^{2+} through the pipette opening at a constant E_{sub}, at least for this range of bias magnitudes. The substrate potential evidently has most effect on feature growth, controlling the

electrochemical kinetics of deposition and to some extent ~~providing~~ leading to a small variation of feature thickness (similar~~ly~~ to deposition with FluidFM probes),[48] while the mass transport of Cu^{2+} ions from the nanopipette is mainly controlled by the bias on the QRCE in the delivery barrel.

Under the conditions ~~given~~ used herein (*i.e.* ~~slightly~~ acidic electrolyte, high salt concentrations) the ion fluxes through the nanopipette follow ohmic behaviour, ~~(straight current-voltage curves, not shown) and do not~~ rather than ~~exhibit~~ diode-like characteristics. This is attributed to the fact that ion current rectification ~~phenomenon~~,[53] which is related to ~~the presence of the~~ surface charge on the conical nanopipette inner walls,[54] is weak as the silanol groups (pK_a around 4.5 and 8.5) on the glass/quartz surface are protonated (neutral charge) as the ~~(~~electrolyte pH is around 2-3,~~)~~ ~~and surface charge magnitude is small,~~ and the rectification effect is further diminished by the high salt concentration (small Debye length).[40]

Figure 3b illustrates the reproducibility of fabrication, showing a set of 9 pillars deposited at different regions of a gold substrate. Deposition rates of 115 nm s^{-1} were reasonably consistent within this set (relative standard deviation of 12%). An electron microscope image at high magnification of one of the fabricated pillars is shown in Figure 3c. As can be seen, the deposit has a fairly uniform thickness from the base to the top. Slight variations of the pillar thickness and shape are most likely due to the polycrystalline nature of the deposit as also seen in pillars deposited by the FluidFM probe.[49] Potentially, the use of surfactants and additives could allow the fabrication of smoother nanoscale features and some tailoring of the aspect ratio. Interestingly, the structure diameter (400 – 600 nm) is about 10 times larger than the opening size of the pipette barrel (30 – 50 nm). In the jet-printing configuration of patterning with FluidFM probes the features patterned were at least three times thicker than the opening diameter

Formatted: Highlight

Formatted: Highlight

Formatted: Subscript

Formatted: Highlight

of the probe.[49] This effect, for both methods, is attributed to the broadening of the interfacial concentration field of the confined precursor species at close probe-to-substrate distances. At least in part, this can be attributed to sluggish deposition kinetics compared to the mass transport rate, especially in relation to the nucleation and growth of copper on gold. The absence of any growth features, other than a deposited layer of copper at low substrate overpotential values (Figure 3a) also supports this hypothesis.

The technique outlined is capable of deposition of more complex 3D structures, which can be used further for optical and nanomechanical applications, as unconventional SPM probes and in nanoelectronic devices as interconnects.[1,55-57] Figure 4a shows two freestanding 25 μm and 27 μm – tall zigzag features (both structures are ~500 nm thick). These structures were grown by the deposition of a vertical pillar (3 μm in height), followed by the copper electroplating with a laterally translated nanopipette at a rate of 50 nm s^{-1}, which allowed the construction of a metal wire in a diagonal configuration, with each diagonal inclined at about 60 degrees with respect to the substrate. These structures arise from the retraction of the nanopipette (positional feedback) with the growing feature (rate of electrodeposition *ca.* 100 nm s^{-1}) and the simultaneous lateral movement of the probe. These two factors determine the geometric characteristics of the resulting 3D shape and could easily be tuned.

Finally, we point out that if positional feedback is turned off at certain points during patterning, and the probe is then translated laterally, Γ-like structures can be deposited. Figure 4b shows a fabricated freestanding Γ feature, consisting of a vertical (5.5 μm height) and horizontal (2.2 μm length) copper wire. Note that this is about an order of magnitude thinner (800 nm in diameter) than a previously reported similar pattern, deposited with the microfluidic hollow AFM cantilever technique.[49]

~~Importantly, t~~The grown complex features were subjected to all the necessary sample manipulation and preparation (thorough rinsing, removal of the substrate~~ing~~ from the sample holder, mounting on the holder for SEM, transfer to SEM) needed for further characterization, and no mechanical damage was observed on the fabricated objects. This confirms the~~a~~ reasonable mechanical stability of the features, which are ~~possibly~~ likely to be mechanically similar to the~~ ones~~ose fabricated by FluidFM.[49]

SICM imaging of fabricated objects

In addition to fine control over surface modification, the nanopipette patterning method presented here also offers the possibility to map the patterned area using the imaging capabilities of the *same probe* as used for fabrication. The advantage of imaging the features ~~right~~ immediately after the fabrication has several important benefits, such as: i) "quality control" after particular~~t~~ preparation steps in the multistep fabrication of complex objects;~~,~~ ii) almost immediate characterization, with a reasonably quick image acquisition time, with no need for~~to~~ *in-situ* sample manipulation/preparation for the use of other characterization techniques; and iii) the possibility of imaging materials that could~~an~~ be changed or ~~/~~modified~~/destroyed~~ outside the fabrication conditions (*e.g.* damaged in ~~the~~ an electron beam, oxidized by oxygen present in the ambient atmosphere *etc*).

Figure 5a shows a 750 nm by 750 nm high-resolution SICM image (2500 pixels, 15 nm pixel pitch) of a copper pillar (as deposited height 2.83 ± 0.08 µm) obtained with a dual-barrel nanopipette of 100 nm total diameter (SICM barrel internal opening size was ~30 nm). A hopping mode was used as described in the methods section. The image demonstrates the elliptic shape of the 2.95 µm µm-tall feature (measured by SICM) with *ca.* 400 and 500 nm dimensions

Formatted: Highlight

along the semi-minor and semi-major axes. The pillar has some roughness on the side walls, similar to the other deposited structures (*e.g.* as in Figure 3c) and this structural characteristic is clearly visualized by SICM. It is important to note that imaging of such three-dimensional objects of high aspect ratio (tall and narrow, with vertical sidewalls) is a challenging task for most SPMs, including AFM, due to steric difficulties attributed to the geometry of the probes. An advantage of SICM probes is their high aspect ratio. We note that the FluidFM probe has a geometry designed for fluid flow, rather than imaging, so that high resolution writing and reading is not possible.

Although SICM imaging with a nanopipette probe is feasible even on structures with such a shape as that shown in Figure 5a, particular care has to be taken to avoid probe-substrate crash. Figures 5b and c exhibit approach curves recorded during SICM topographical mapping. A classical SICM current-distance characteristic[50] (Figure 5b) is recorded over the flat featureless part of the substrate (pixel marked "b" in Figure 5a). Similar current-distance curves are recorded on the central part of the pillar (not shown). However, the current-distance response over the edges of the copper structure (*e.g.* marked "c" in Figure 5a) is rather different. Figure 5c shows such a current-distance characteristic, which exhibits two minima, one below the feedback set point (at the position of closest approach, 0 μm on the graph) and another slightly above the set point value (at a probe-to-substrate distance *ca*. 2.5 μm). The former minimum most likely indicates the vicinity of the probe to the flat part of the substrate, similar to the classical ion current response over the planar interface (as illustrated on Figure 5d). The latter minimum is attributed to the ion current magnitude drop due to the steric limitation of the mass-transport in close proximity to the pillar (*i.e.* a vertical wall). The gradual flattening of the minimum indicates the change of the mutual arrangement of the nanopipette tip and the deposited structure

and is most likely due to nanopipette bending. Indeed, this scenario is quite possible, taking into account the nanopipette semi-angle (about 8°) and the distance between pixels (15 nm), which means that mechanical contact between the probe and the copper pillar can be established (as shown schematically in Figure 5e), causing further probe/structure bending during the approach. Despite this issue, the SICM channel of the dual-function probe can generally be used for post-fabrication read-out of the deposited features.

CONCLUSIONS

This work has demonstrated the capabilities of double-barrel nanopipettes for highly controlled deposition of 3D structures, using Cu deposition as an exemplar material. The methodology is based on the electrochemical management of ionic fluxes for highly localized electrochemically-driven delivery and deposition, as well as for ion conductance regulation of the probe-to-substrate distance. This approach has been illustrated with the fabrication of simple (pillars) and more complex objects, such as free-standing zigzag and Γ-like structures. Advantages of the nanopipette technique include relatively straightforward operation, simple electrochemical control of delivery (without any need for a flow system), with simultaneous monitoring and feedback, and facile adjustment of the deposition parameters and growth rates by simultaneous tuning of the bias that drives precursor ions and the substrate potential.

As well as being able to produce (write) features, the same probe can be used to image (read) the deposited features using the powerful high-resolution imaging capacity of SICM. Furthermore, any difficulties of surface wettability and stability of meniscus-confined methods are overcome by operation under a thick layer of electrolyte solution. In principle, the technique should be capable of using the voxel-by-voxel fabrication strategy reported previously for the

fabrication of even more complex object architectures[49] and should be compatible with the electroplating of a variety of materials, spanning conducting polymers, nanoparticles and metals. In this regard, it is important to point out the ease with which multi-barrel pipettes can be constructed,[58] which would enable the construction of multi-component structures, of spatially varying composition if desired, via (adaptive) potential-space-time control.

METHODS

Chemicals

Sodium sulfate (anhydrous, analytical grade, Fisher Scientific), copper sulfate (technical grade, Fisons Scientific Equipment) and sulfuric acid (≥95%, density 1.83 g ml^{-1}, analytical reagent grade, Fisher Scientific,) were used as received. Deionized (DI) water produced by Purite Select HP system, with resistivity 18.2 MΩ cm (25 °C) was used to prepare aqueous solutions. Electrolyte solution in the bulk and in the SICM pipette barrel contained Na_2SO_4 (0.5 M) and H_2SO_4 (3 mM), while the nanopipette barrel used as a source of copper ions (Cu^{2+}) was filled with $CuSO_4$ (56 – 270 mM) and H_2SO_4 (3 – 100 mM).

Nanopipette probes

Nanopipettes were pulled from dual-barrel quartz capillaries with filament (QTF120-90-100, Friedrich & Dimmock) using a laser pipette puller (P-2000, Sutter Instruments). Nanopipette probes were filled with electrolyte solutions using syringes with Microfill capillaries MF34G-5 (World Precision Instruments). Importantly, the nanopipette filling process does not cause significant cross-contamination between the different electrolytes in the nanopipette barrels (from a small liquid droplet that can form at the tip) ~~a~~to any significant level (see Supporting

Information, SI-1). Geometric characterization of nanopipette probes was carried out on either gold-coated pipette tips imaged with a field-emission scanning electron microscope (FE-SEM, Zeiss SUPRA 55 VP) or on uncoated nanopipette tips, with geometries determined at high resolution[52,59] using a transmission electron microscope (TEM) JEOL 2000FX at 200 kV accelerating voltage.

Scanning ion conductance microscopy (SICM) setup

Nanopipette probes, mounted on a custom made probe holder, were coarsely positioned over a sample with a mechanical micropositioner (Newport, M-461-XYZ-M) under control of a 3MP digital camera (PixeLink PL-B776U) with a 4X magnification lens. A 38 μm-range single axis nanopositioner (Physik Instrumente, P-753.3CD) was used for precise control and translation of the probe in the vertical (z) direction (normal to the substrate). A small vertical oscillation of the probe (40 nm peak-to-peak) at a frequency typically in the range 270 – 290 Hz was applied using a lock-in amplifier (Stanford Research Systems, SR830). This induced an alternating current (AC), the magnitude of which served as positional feedback (distance-modulated SICM).[60,61] In general, AC-SICM techniques provide very stable probe positioning.[60,61] The sample, 60 nm gold thin film on 3 nm chromium layer deposited on silicon wafer, with an exposed to electrolyte solution surface area of about 3 mm^2, was biased using a custom built bipotentiostat. The sample was mounted on the stage of an inverted microscope equipped with a high-precision XY nanopositioning piezoelectric stage (MadCityLabs, Nano-Bio300 and Physik Instrumente, model P-733.2DD). The setup was mounted inside a faraday cage (to reduce electrical noise), which was built on an optical table (Newport, RS 2000) to avoid mechanical vibrations. To reduce thermal drift of the piezoelectric positioners, vacuum insulating panels (Kevothermal) and aluminium heat sinks were mounted inside the faraday cage. Electrochemical measurements

were performed with a custom-built bipotentiostat equipped with a high sensitivity current follower to measure nanopipette probe currents from both channels. The SICM setup was controlled through an FPGA card (PCIe-7852R, National Instruments) using a home-written program in a LabVIEW interface that was also used for all data acquisition.

REFERENCES

1. Hu, J.; Yu, M.-F. Meniscus-Confined Three-Dimensional Electrodeposition for Direct Writing of Wire Bonds. *Science* **2010**, 329, 313-316.
2. Stewart, M. E.; Anderton, C. R.; Thompson, L. B.; Maria, J.; Gray, S. K.; Rogers, J. A.; Nuzzo, R. G. Nanostructured Plasmonic Sensors. *Chem. Rev. (Washington, DC, U. S.)* **2008**, 108, 494-521.
3. Xiang, Z.; Liu, J.; Lee, C. A Flexible Three-Dimensional Electrode Mesh: an Enabling Technology for Wireless Brain–Computer Interface Prostheses. *Microsystems & Nanoengineering* **2016**, 2, 16012.
4. Meng, D.; Erol, M.; Boccaccini, A. R. Processing Technologies for 3D Nanostructured Tissue Engineering Scaffolds. *Adv. Eng. Mater.* **2010**, 12, B467-B487.
5. Li, J.; Rozen, I.; Wang, J. Rocket Science at the Nanoscale *ACS Nano*, **2016**, DOl: 10.1021/acsnano.6b02518.
6. De Angelis, F.; Malerba, M.; Patrini, M.; Miele, E.; Das, G.; Toma, A.; Zaccaria, R. P.; Di Fabrizio, E. 3D Hollow Nanostructures as Building Blocks for Multifunctional Plasmonics. *Nano Lett.* **2013**, 13, 3553-3558.
7. Yesilkoy, F.; Flauraud, V.; Ruegg, M.; Kim, B. J.; Brugger, J. 3D Nanostructures Fabricated by Advanced Stencil Lithography. *Nanoscale* **2016**, 8, 4945-4950.
8. Jesse, S.; Borisevich, A. Y.; Fowlkes, J. D.; Lupini, A. R.; Rack, P. D.; Unocic, R. R.; Sumpter, B. G.; Kalinin, S. V.; Belianinov, A.; Ovchinnikova, O. S. Directing Matter: Toward Atomic-Scale 3D Nanofabrication *ACS Nano*, **2016**, DOl: 10.1021/acsnano.6b02489.
9. Fisher, J. S.; Kottke, P. A.; Kim, S.; Fedorov, A. G. Rapid Electron Beam Writing of Topologically Complex 3D Nanostructures Using Liquid Phase Precursor. *Nano Lett.* **2015**, 15, 8385-8391.
10. Ke, Y.; Ong, L. L.; Shih, W. M.; Yin, P. Three-Dimensional Structures Self-Assembled from DNA Bricks. *Science* **2012**, 338, 1177-1183.
11. Han, D.; Pal, S.; Nangreave, J.; Deng, Z.; Liu, Y.; Yan, H. DNA Origami with Complex Curvatures in Three-Dimensional Space. *Science* **2011**, 332, 342-346.
12. Meyer, E.; Hug, H. J.; Bennewitz, R. Introduction to Scanning Tunneling Microscopy. In *Scanning Probe Microscopy: The Lab on a Tip*, Springer Berlin Heidelberg: Berlin, Heidelberg, 2004; pp 15-44.
13. Iwata, F.; Metoki, J. In *Microelectrophoresis Deposition Using a Nanopipette for Three-Dimensional Structures*, Manipulation, Manufacturing and Measurement on the Nanoscale (3M-NANO), 2014 International Conference on, 27-31 Oct. 2014; 2014; pp 304-307.
14. Resch, R.; Baur, C.; Bugacov, A.; Koel, B. E.; Madhukar, A.; Requicha, A. A. G.; Will, P. Building and Manipulating Three-Dimensional and Linked Two-Dimensional Structures of Nanoparticles Using Scanning Force Microscopy. *Langmuir* **1998**, 14, 6613-6616.
15. Zhao, J.; Swartz, L. A.; Lin, W.-f.; Schlenoff, P. S.; Frommer, J.; Schlenoff, J. B.; Liu, G.-y. Three-Dimensional Nanoprinting via Scanning Probe Lithography-Delivered Layer-by-Layer Deposition. *ACS Nano* **2016**.
16. Pires, D.; Hedrick, J. L.; De Silva, A.; Frommer, J.; Gotsmann, B.; Wolf, H.; Despont, M.; Duerig, U.; Knoll, A. W. Nanoscale Three-Dimensional Patterning of Molecular Resists by Scanning Probes. *Science* **2010**, 328, 732-735.
17. El-Giar, E. M.; Said, R. A.; Bridges, G. E.; Thomson, D. J. Localized Electrochemical Deposition of Copper Microstructures. *J. Electrochem. Soc.* **2000**, 147, 586-591.

18. McGeouch, C.-A.; Peruffo, M.; Edwards, M. A.; Bindley, L. A.; Lazenby, R. A.; Mbogoro, M. M.; McKelvey, K.; Unwin, P. R. Quantitative Localized Proton-Promoted Dissolution Kinetics of Calcite Using Scanning Electrochemical Microscopy (SECM). *J. Phys. Chem. C* **2012**, 116, 14892-14899.
19. Borgwarth, K.; Heinze, J. Increasing the Resolution of the Scanning Electrochemical Microscope Using a Chemical Lens: Application to Silver Deposition. *J. Electrochem. Soc.* **1999**, 146, 3285-3289.
20. Laslau, C.; Williams, D. E.; Kannan, B.; Travas-Sejdic, J. Scanned Pipette Techniques for the Highly Localized Electrochemical Fabrication and Characterization of Conducting Polymer Thin Films, Microspots, Microribbons, and Nanowires. *Adv. Funct. Mater.* **2011**, 21, 4607-4616.
21. Kim, J. T.; Seol, S. K.; Pyo, J.; Lee, J. S.; Je, J. H.; Margaritondo, G. Three-Dimensional Writing of Conducting Polymer Nanowire Arrays by Meniscus-Guided Polymerization. *Adv. Mater.* **2011**, 23, 1968-1970.
22. Bruckbauer, A.; Ying, L.; Rothery, A. M.; Zhou, D.; Shevchuk, A. I.; Abell, C.; Korchev, Y. E.; Klenerman, D. Writing with DNA and Protein Using a Nanopipet for Controlled Delivery. *J. Am. Chem. Soc.* **2002**, 124, 8810-8811.
23. Bruckbauer, A.; Zhou, D.; Ying, L.; Korchev, Y. E.; Abell, C.; Klenerman, D. Multicomponent Submicron Features of Biomolecules Created by Voltage Controlled Deposition from a Nanopipet. *J. Am. Chem. Soc.* **2003**, 125, 9834-9839.
24. Iwata, F.; Nagami, S.; Sumiya, Y.; Sasaki, A. Nanometre-Scale Deposition of Colloidal Au Particles Using Electrophoresis in a Nanopipette Probe. *Nanotechnology* **2007**, 18, 105301.
25. So, I.; Futoshi, I. Nanometer-Scale Deposition of Metal Plating Using a Nanopipette Probe in Liquid Condition. *Jpn. J. Appl. Phys.* **2011**, 50, 08LB15.
26. Abhijit, P. S.; Min-Feng, Y. Electrochemical Fountain Pen Nanofabrication of Vertically Grown Platinum Nanowires. *Nanotechnology* **2007**, 18, 105305.
27. Zhou, M.; Yu, Y.; Blanchard, P.-Y.; Mirkin, M. V. Surface Patterning Using Diazonium Ink Filled Nanopipette. *Anal. Chem.* **2015**, 87, 10956-10962.
28. Suryavanshi, A. P.; Yu, M.-F. Probe-based Electrochemical Fabrication of Freestanding Cu Nanowire Array. *Appl. Phys. Lett.* **2006**, 88, 083103.
29. Müller, A.-D.; Müller, F.; Hietschold, M. Electrochemical Pattern Formation in a Scanning Near-Field Optical Microscope. *Applied Physics A* **1998**, 66, S453-S456.
30. Müller, A. D.; Müller, F.; Hietschold, M. Localized Electrochemical Deposition of Metals Using Micropipettes. *Thin Solid Films* **2000**, 366, 32-36.
31. Zhang, H.; Wu, L.; Huang, F. Electrochemical Microprocess by Scanning Ion-Conductance Microscopy. *J. Vac. Sci. Technol., B: Microelectron. Nanometer Struct.--Process., Meas., Phenom.* **1999**, 17, 269-272.
32. Lesch, A.; Vaske, B.; Meiners, F.; Momotenko, D.; Cortes-Salazar, F.; Girault, H. H.; Wittstock, G. Parallel Imaging and Template-Free Patterning of Self-Assembled Monolayers with Soft Linear Microelectrode Arrays. *Angew. Chem., Int. Ed.* **2012**, 51, 10413-10416.
33. ul Haq, E.; Liu, Z. M.; Zhang, Y. A.; Ahmad, S. A. A.; Wong, L. S.; Armes, S. P.; Hobbs, J. K.; Leggett, G. J.; Micklefield, J.; Roberts, C. J., *et al*. Parallel Scanning Near-Field Photolithography: The Snomipede. *Nano Lett.* **2010**, 10, 4375-4380.
34. Vettiger, P.; Despont, M.; Drechsler, U.; Durig, U.; Haberle, W.; Lutwyche, M. I.; Rothuizen, H. E.; Stutz, R.; Widmer, R.; Binnig, G. K. The "Millipede" - More than Thousand Tips for Future AFM Storage. *IBM J. Res. Dev.* **2000**, 44, 323-340.

Formatted: Highlight

35. Loh, O. Y.; Ho, A. M.; Rim, J. E.; Kohli, P.; Patankar, N. A.; Espinosa, H. D. Electric Field-Induced Direct Delivery of Proteins by a Nanofountain Probe. *Proc. Natl. Acad. Sci. U. S. A.* **2008**, 105, 16438-16443.
36. Aaronson, B. D. B.; Güell, A. G.; McKelvey, K.; Momotenko, D.; Unwin, P. R. Scanning Electrochemical Cell Microscopy: Mapping, Measuring, and Modifying Surfaces and Interfaces at the Nanoscale. In *Nanoelectrochemistry*, CRC Press: 2015; pp 655-694.
37. Kang, M.; Momotenko, D.; Page, A.; Perry, D.; Unwin, P. R. Frontiers in Nanoscale Electrochemical Imaging: Faster, Multifunctional and Ultrasensitive *Langmuir*, **2016**, DOl: 10.1021/acs.langmuir.6b01932.
38. Momotenko, D.; McKelvey, K.; Kang, M.; Meloni, G. N.; Unwin, P. R. Simultaneous Interfacial Reactivity and Topography Mapping with Scanning Ion Conductance Microscopy. *Anal. Chem.* **2016**, 88, 2838-2846.
39. Momotenko, D.; Byers, J. C.; McKelvey, K.; Kang, M.; Unwin, P. R. High-Speed Electrochemical Imaging. *ACS Nano* **2015**, 9, 8942-8952.
40. Perry, D.; Al Botros, R.; Momotenko, D.; Kinnear, S. L.; Unwin, P. R. Simultaneous Nanoscale Surface Charge and Topographical Mapping. *ACS Nano* **2015**, 9, 7266-7276.
41. McKelvey, K.; Kinnear, S. L.; Perry, D.; Momotenko, D.; Unwin, P. R. Surface Charge Mapping with a Nanopipette. *J. Am. Chem. Soc.* **2014**, 136, 13735-13744.
42. Perry, D.; Paulose Nadappuram, B.; Momotenko, D.; Voyias, P. D.; Page, A.; Tripathi, G.; Frenguelli, B. G.; Unwin, P. R. Surface Charge Visualization at Viable Living Cells. *J. Am. Chem. Soc.* **2016**, 138, 3152-3160.
43. McKelvey, K.; O'Connell, M. A.; Unwin, P. R. Meniscus Confined Fabrication of Multidimensional Conducting Polymer Nanostructures With Scanning Electrochemical Cell Microscopy (SECCM). *Chem. Commun.* **2013**, 49, 2986-2988.
44. Rodolfa, K. T.; Bruckbauer, A.; Zhou, D.; Korchev, Y. E.; Klenerman, D. Two-Component Graded Deposition of Biomolecules with a Double-Barreled Nanopipette. *Angew. Chem., Int. Ed.* **2005**, 44, 6854-6859.
45. An, S.; Sung, B.; Noh, H.; Stambaugh, C.; Kwon, S.; Lee, K.; Kim, B.; Kim, Q.; Jhe, W. Position-resolved Surface Characterization and Nanofabrication Using an Optical Microscope Combined with a Nanopipette/Quartz Tuning Fork Atomic Force Microscope. *Nano-Micro Letters* **2014**, 6, 70-79.
46. Futoshi, I.; Yosuke, S.; Akira, S. Nanometer-Scale Metal Plating Using a Scanning Shear-Force Microscope with an Electrolyte-Filled Micropipette Probe. *Jpn. J. Appl. Phys.* **2004**, 43, 4482.
47. Meister, A.; Gabi, M.; Behr, P.; Studer, P.; Vörös, J.; Niedermann, P.; Bitterli, J.; Polesel-Maris, J.; Liley, M.; Heinzelmann, H*., et al.* FluidFM: Combining Atomic Force Microscopy and Nanofluidics in a Universal Liquid Delivery System for Single Cell Applications and Beyond. *Nano Lett.* **2009**, 9, 2501-2507.
48. Hirt, L.; Gruter, R. R.; Berthelot, T.; Cornut, R.; Voros, J.; Zambelli, T. Local Surface Modification via Confined Electrochemical Deposition with FluidFM. *RSC Advances* **2015**, 5, 84517-84522.
49. Hirt, L.; Ihle, S.; Pan, Z.; Dorwling-Carter, L.; Reiser, A.; Wheeler, J. M.; Spolenak, R.; Vörös, J.; Zambelli, T. Template-Free 3D Microprinting of Metals Using a Force-Controlled Nanopipette for Layer-by-Layer Electrodeposition. *Adv. Mater.* **2016**, 28, 2311-2315.
50. Chen, C.-C.; Zhou, Y.; Baker, L. A. Scanning Ion Conductance Microscopy. *Annu. Rev. Anal. Chem.* **2012**, 5, 207-228.

51. Hansma, P. K.; Drake, B.; Marti, O.; Gould, S. A.; Prater, C. B. The Scanning Ion-Conductance Microscope. *Science* **1989**, 243, 641-3.
52. Perry, D.; Momotenko, D.; Lazenby, R. A.; Kang, M.; Unwin, P. R. Characterization of Nanopipettes. *Anal. Chem.* **2016**, 88, 5523-5530.
53. Wei, C.; Bard, A. J.; Feldberg, S. W. Current Rectification at Quartz Nanopipet Electrodes. *Anal. Chem.* **1997**, 69, 4627-4633.
54. Momotenko, D.; Cortés-Salazar, F.; Josserand, J.; Liu, S.; Shao, Y.; Girault, H. H. Ion Current Rectification and Rectification Inversion in Conical Nanopores: a Perm-Selective View. *Phys. Chem. Chem. Phys.* **2011**.
55. Butt, F. K.; Cao, C.; Khan, W. S.; Safdar, M.; Fu, X.; Tahir, M.; Idrees, F.; Ali, Z.; Nabi, G.; Yu, D. Electrical and Optical Properties of Single Zigzag SnO2 Nanobelts. *CrystEngComm* **2013**, 15, 2106-2112.
56. Zhou, X. T.; Sham, T. K.; Shan, Y. Y.; Duan, X. F.; Lee, S. T.; Rosenberg, R. A. One-Dimensional Zigzag Gallium Nitride Nanostructures. *J. Appl. Phys.* **2005**, 97, 104315.
57. Göring, G.; Dietrich, P.-I.; Blaicher, M.; Sharma, S.; Korvink, J. G.; Schimmel, T.; Koos, C.; Hölscher, H. Tailored Probes for Atomic Force Microscopy Fabricated by Two-Photon Polymerization. *Appl. Phys. Lett.* **2016**, 109, 063101.
58. Nadappuram, B. P.; McKelvey, K.; Byers, J. C.; Güell, A. G.; Colburn, A. W.; Lazenby, R. A.; Unwin, P. R. Quad-Barrel Multifunctional Electrochemical and Ion Conductance Probe for Voltammetric Analysis and Imaging. *Anal. Chem.* **2015**, 87, 3566-3573.
59. Sa, N.; Baker, L. A. Experiment and Simulation of Ion Transport through Nanopipettes of Well-Defined Conical Geometry. *J. Electrochem. Soc.* **2013**, 160, H376-H381.
60. Shevchuk, A. I.; Gorelik, J.; Harding, S. E.; Lab, M. J.; Klenerman, D.; Korchev, Y. E. Simultaneous Measurement of Ca2+ and Cellular Dynamics: Combined Scanning Ion Conductance and Optical Microscopy to Study Contracting Cardiac Myocytes. *Biophys. J.* **2001**, 81, 1759-1764.
61. Li, C.; Johnson, N.; Ostanin, V.; Shevchuk, A.; Ying, L.; Korchev, Y.; Klenerman, D. High Resolution Imaging Using Scanning Ion Conductance Microscopy with Improved Distance Feedback Control. *Prog. Nat. Sci.* **2008**, 18, 671-677.

Formatted: Highlight

Commented [AP1]: Reference 54 also incomplete

Commented [AP2]: Reference 15 incomplete, add DOI if not yet published

Commented [AP3]: I have highlighted what I think are the new refs because Pat wants them highlighted – please check that I've got them all and that I haven't highlighted any that were already in the manuscript

ACKNOWLEDGMENT

This work was supported by a Marie Curie IntraEuropean Fellowship 626158 FUNICIS (D.M.), a Marie Curie Initial Training Network FP7-People-2012-ITN Grant Agreement Number 316630 CAS-IDP (M. A.-V.) and the EPSRC through the MOAC DTC, grant no. EP/F500378/1 (A.P.). The authors thank Minkyung Kang for TEM imaging of the nanopipette probes.

COMPETING FINANCIAL INTERESTS

The authors declare no competing financial interests.

FIGURES

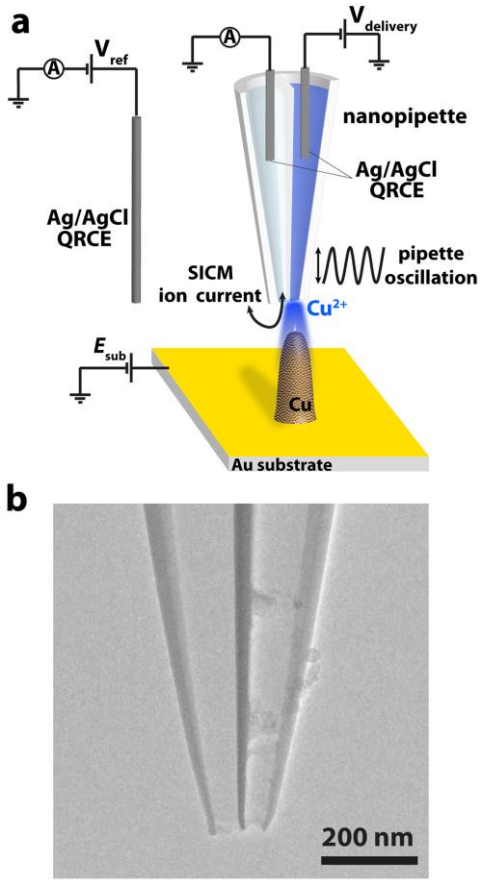

Figure 1. a) Schematic representation of the experimental setup employed for deposition of 3D high aspect ratio Cu features on a gold electrode surface. b) TEM image of a typical dual-barrel nanopipette probe used for nanoscale patterning with SICM positional feedback.

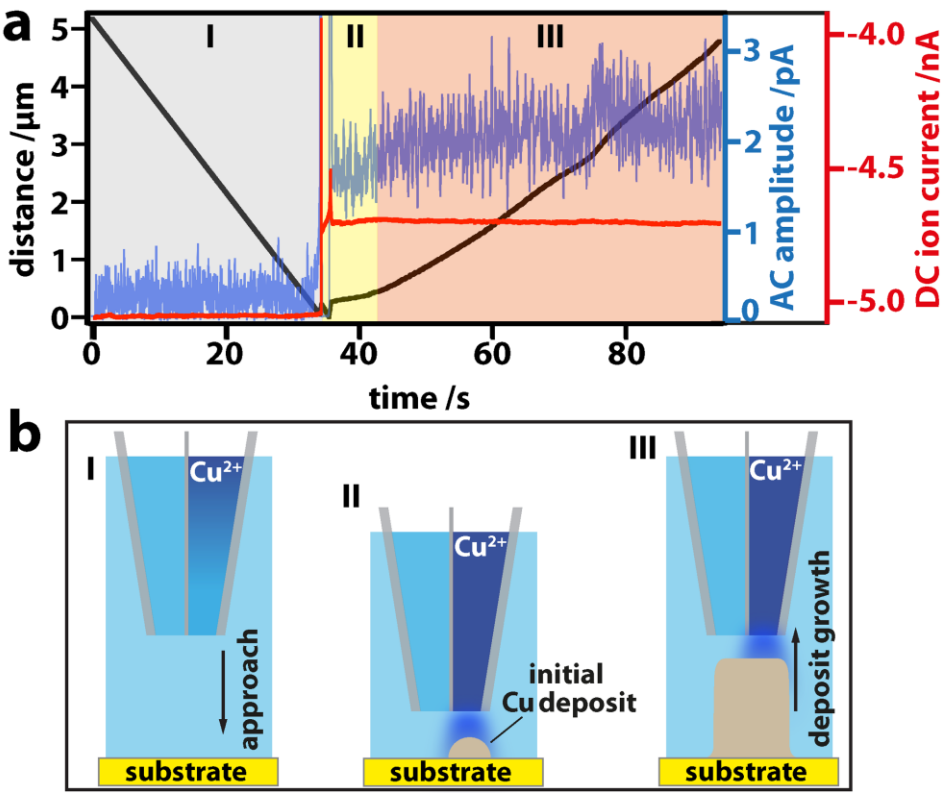

Figure 2. a) Variation with time of the probe vertical position (black), pipette AC and DC ion currents (for the barrel employed for distance control; blue and red, respectively) during the growth of a Cu pillar on a gold substrate. The data reveal the following: I) approach of the probe to the substrate at a rate of 150 nm s^{-1} (negative bias of -0.2 V applied to the pipette barrel containing Cu^{2+}) with a stable (bulk) DC ion current (SICM bias -0.2 V) and zero AC amplitude. II) The DC current shows a steep decline over a distance of ~200 nm inducing an increase in AC amplitude. Having reached the AC amplitude set point there is commencement of the deposition of an initial ~100 nm section of the Cu pillar following a switch of the Cu^{2+} delivery channel to 1

V. III) Growth of the deposit in the vertical direction with the AC amplitude maintained slightly above 1.5 pA and the DC ion current value being consistent for the whole duration of the deposition. The probe retracts from the surface as the Cu pillar grows and the rate of tip movement is the growth rate. Note that the images are not to scale (*i.e.* the deposit under the nanopipette is usually 10 times larger than the ~~barrels~~ opening size of a channel in the nanopipette). The color code on the ordinate axes corresponds to the line colors on the graph. Schematic illustrations in (b) depict the position of the pipette with respect to substrate and the growing deposit feature during patterning.

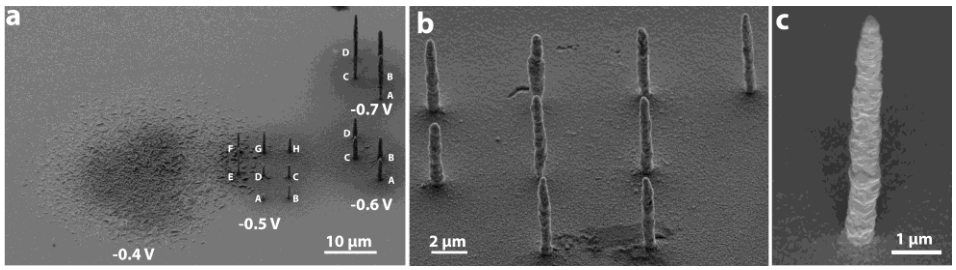

Figure 3. SEM micrographs (taken at a 45° inclination angle) of copper pillars patterned on gold substrates. a) The effect of the substrate potential on deposition. Features at substrate potentials of -0.4 V and -0.5 V contained eight depositions, while arrays grown at E_{sub} = -0.6 V and E_{sub} = -0.7 V consisted of four individual pillars. The bias in the $CuSO_4$-filled barrel was between 0.3 V and 1V for substrate potentials of -0.4 V and -0.5 V (marked from "A" to "H") and from 0.8 to 1.1 V (in 0.1 V increments, "A" to "D") for substrate potentials of -0.6 V and -0.7 V. The SICM bias was fixed at -0.25 V and the deposition time was set to 180 s. b) An array of nine pillars deposited at E_{sub} = -0.75 V, SICM bias 0.2 V and the bias in a copper reservoir barrel of 1 V. Deposition time was set to 60 s. c) A magnified view of one of the pillars, deposited under similar conditions as in (b), except that the bias value in the copper-containing pipette barrel was 1.2 V.

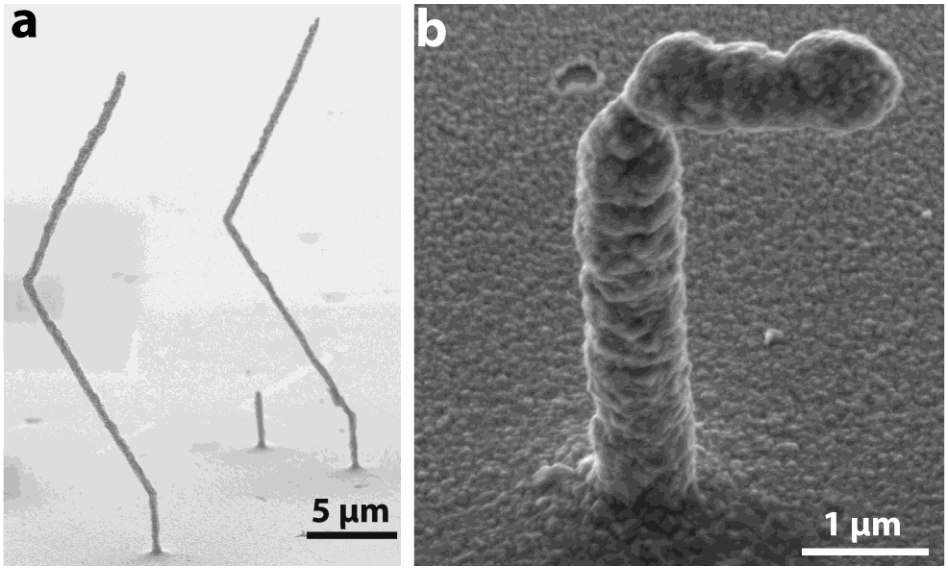

Figure 4. SEM images of complex 3D features fabricated with a dual-channel nanopipette. a) Two zigzag structures, created by driving Cu^{2+} ions from the delivery channel at a bias of +0.7 V with positional SICM feedback (image taken at a 15° angle). The vertical pillar at the structure base was fabricated by holding the nanopipette for 45 s above the substrate (*i.e.* fixed x, y co-ordinate; feedback on z-position). Diagonal parts of the structure were deposited by translating the nanopipette for 6 µm laterally at 50 nm s^{-1}. b) Fabricated Γ-like feature (image taken at a 45° angle), deposited at 0.75 V driving voltage. The top bar of the Γ was deposited by translating the nanopipette probe laterally at 40 nm s^{-1} without SICM positional feedback. The substrate was held at a potential E_{sub} = -0.75 V throughout. SICM barrels in both deposition experiments were biased at 0.2 V *vs.* QRCE in the solution bulk.

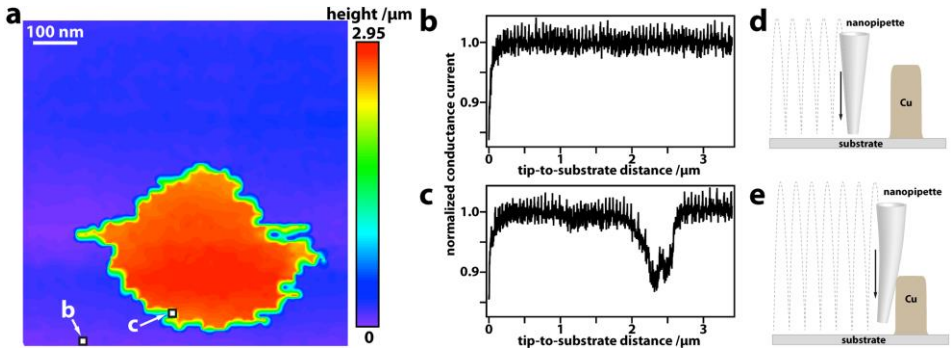

Figure 5. a) Hopping mode SICM image (750 by 750 nm, 2500 pixels, 15 nm pixel pitch) of a deposited Cu pillar, taken with the *same nanopipette probe* as used for patterning (deposition at E_{sub} =-0.75 V, SICM bias 0.2 V, copper-barrel bias 0.7 V, 60 s). b), c) Probe approach curves recorded at positions "b" and "c" as marked on (a). Schematics in (d) and (e) illustrate possible nanopipette bending in (b) and (c), respectively.

For TOC only

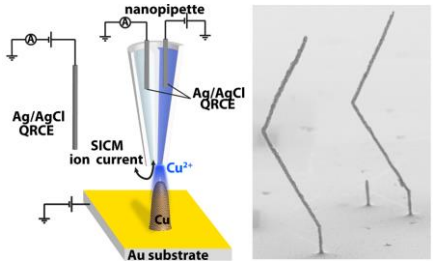
nanopipette
Ag/AgCl QRCE
Ag/AgCl QRCE
SICM ion current
Cu2+
Cu
Au substrate